Influence of transition-metal type and content on local-order properties of $Zn_{1-x}M_xS$ (M = Mn,Fe,Co) alloys studied using XANES spectroscopy

W. F. Pong
Department of Physics, Tamkang University, Tamsui, Taiwan 251, Republic of China

R. A. Mayanovic
Department of Physics and Astronomy, Southwest Missouri State University, Springfield, Missouri 65804

K. T. Wu and P. K. Tseng
Department of Physics, National Taiwan University, Taipei, Taiwan 107, Republic of China

B. A. Bunker
Department of Physics, University of Notre Dame, Notre Dame, Indiana 46556

A. Hiraya and M. Watanabe
Institute for Molecular Science, Myodaiji, Okzaki 444, Japan
(Received 6 August 1993; revised manuscript received 5 May 1994)

X-ray-absorption near-edge-structure (XANES) spectra of the diluted-magnetic-semiconductor system $Zn_{1-x}Mn_xS$ have been measured at the Zn $L_{III,II}$ edge and of $Zn_{1-x}M_xS$ (M = Mn,Fe,Co) at the S K edge using the total-electron-yield mode. The Zn L_{III} edge results for $Zn_{1-x}Mn_xS$ show a dramatic reduction in intensity of the first prominent feature, just above the edge, in the XANES spectra. Analysis of the S K-edge XANES spectra for $Zn_{1-x}M_xS$ revealed the appearance of a pre-edge peak, having linear x dependence in intensity and assigned to S $1s$ photoelectron excitations to an empty narrow band of S $3p$–M $3d(t_2)$ hybridized antibonding states. The rate of peak intensity with M concentration is associated with differences in the degree of p-d hybridization of states between the transition metal and sulfur. Features above the edge are generally found to decrease in intensity with an increase in transition-metal content in the alloys. The results are consistent with more S $3p$–transition metal (M) $3d(t_2)$ hybridized states and less S $3p$–Zn $4(s,p)$ and S $3p$–Zn $3d$ hybridized states becoming available as the transition-metal content increases in the alloys.

I. INTRODUCTION

Diluted magnetic semiconductors (DMS's) are a group of materials for which a transition metal with a magnetic ion is alloyed with a semiconductor; generally a II-VI compound. The magnetic ion substitutes for the cation during the growth phase. The most widely studied II-VI-based DMS's have been those containing Mn^{2+} as the substitutional magnetic cation. In recent years, Fe- and Co-based DMS's have also been successfully grown and investigated. As a result of alloying transition metal and semiconducting compounds, DMS's exhibit unique electrical, magnetic, and optical properties, many of which can be attributed to the short-range exchange interactions between the spins of the magnetic ions and between the magnetic ions and group-VI anion sp-band electrons.[1] Larson and co-workers[2,3] and Spalek *et al.*[4] theoretically investigated the nature of the short-range exchange mechanisms in DMS's and determined that the magnetic spins interact (antiferromagnetically) predominantly via superexchange, a process involving virtual excitations of valence electrons in Mn $3d$ and anion p orbitals. We have successfully used extended x-ray-absorption fine-structure (EXAFS) techniques in the past to study relationships between certain physical properties of DMS's and their local alloy structure. In an earlier study,[5] we observed a linear x dependence for the distortion of the Mn^{2+}-Se^{-2}-Mn^{2+} tetrahedral bond angle in $Zn_{1-x}Mn_xSe$ which we interpreted as being evidence for the superexchange integral J_{dd} being x dependent. Also, in a subsequent EXAFS study on bond relaxation and structural stability in the $Hg_{1-x}Cd_xTe$ and $Hg_{1-x}Mn_xTe$ ternary alloys,[6] we found evidence for tetrahedral bond weakening in these and other Mn-based DMS alloys, which can be attributed to Mn $3d$- and anion valence p-orbital hybridization, resulting in a decreased amount of charge available for the making of sp^3 bonds.

While EXAFS techniques make use of structure from 30–50 eV and above the absorption edge, there is also very useful structural information in the x-ray-absorption near-edge structure (XANES) region below 30–50 eV.[7,8] A feature inherent in XANES which EXAFS does not possess is information about the partial density of unoccupied states. For x-ray energies in the XANES region, the excited photoelectron undergoes transitions from the core state to an unoccupied state just above the Fermi level, the final state being determined in relation to the initial state by the dipole selection rule (e.g., if the initial

state has s symmetry, the final state must have p symmetry). In DMS's, XANES involves photoelectrons undergoing transitions to unoccupied localized and delocalized states, some of which may be involved in the magnetic cation $3d$- and anion p-orbital hybridization. In this paper, we present our results for XANES studies on the $Zn_{1-x}M_xS$ (M=Mn,Fe,Co) system, showing how the spectra vary as a function of type and content of magnetic ion making up the alloy.

II. EXPERIMENTAL

XANES spectra of $Zn_{1-x}Mn_xS$ have been measured at the Zn $L_{III,II}$ edge and $Zn_{1-x}M_xS$ (M=Mn,Fe,Co) at the S K edge at the Ultraviolet Synchrotron Orbital Radiation Facility (UVSOR), Institute for Molecular Science, Okazaki, Japan, using beam line 7A with an electron-beam energy of 750 MeV and a maximum stored current of 200 mA. The concentrations for the $Zn_{1-x}Mn_xS$ alloy samples were x=0.05, 0.10, 0.20, 0.30, 0.50, and 0.60; for $Zn_{1-x}Fe_xS$ x=0.10, 0.20, 0.30, and 0.50; and for $Zn_{1-x}Co_xS$ x=0.05, 0.10, 0.30, and 0.50. The samples were measured using total-electron-yield mode, with an electron multiplier, under a base pressure of better than 5×10^{-8} torr. Data were collected using beryl ($10\bar{1}0$) and Ge (111) double-crystal monochromators for the Zn $L_{III,II}$ edge and S K edge, respectively. Photon energies were calibrated using the K edge of Al (1567.7 eV) in the beryl crystals for Zn $L_{III,II}$-edge measurements and the M_5 edge (2220 eV) of a Au photocathode for S K-edge measurements, respectively. The $Zn_{1-x}Mn_xS$ samples were grown using Bridgman's technique while the $Zn_{1-x}Fe_xS$ and $Zn_{1-x}Co_xS$ were grown using the chemical vapor transport method. The single phase of the samples was confirmed using x-ray diffraction analysis. The samples were ground using ceramic tools, then sieved to fine powders to 400 mesh (each having particle size <38 μm in diameter) and rubbed onto ultrahigh-vacuum-compatible Scotch Magnetic tape (3M, Cat. No. 182). A single layer of sample on tape was exposed at approximately 45° to the incident beam direction, while the electron-yield detector was oriented approximately 90° to the incident beam direction. The energy resolution was better than 0.5 for beryl and 1.2 eV for Ge-crystal monochromators, respectively. All measurements were performed at room temperature.

III. RESULTS AND DISCUSSIONS

We first present our results for the Zn $L_{III,II}$-edge XANES spectra of $Zn_{1-x}Mn_xS$ and subsequently for the S K-edge XANES spectra for the $Zn_{1-x}M_xS$ (M=Mn,Fe,Co) systems.

Zinc $L_{III,II}$-edge XANES spectra

The Zn $L_{III,II}$-edge XANES spectra of $Zn_{1-x}Mn_xS$ are presented in Fig. 1 After pre-edge background subtraction, the spectra were shifted to the absorption threshold (the spectra are proportional to the incident intensity I_0). Zero energy was set at the Zn L_{III} edge, which was

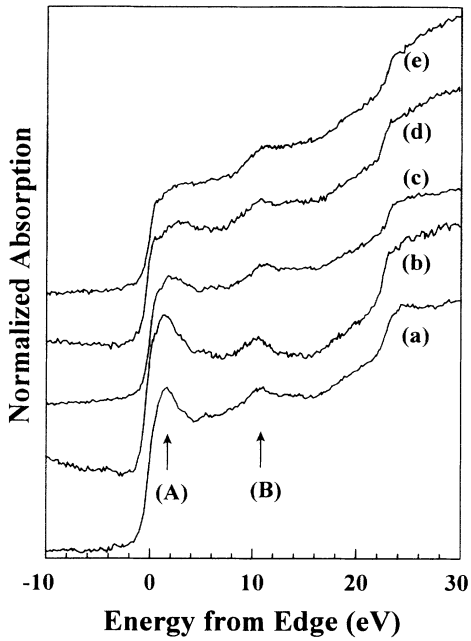

FIG. 1. Zn $L_{III,II}$ near-edge absorption spectra. (a) ZnS, (b) $Zn_{0.8}Mn_{0.2}S$, (c) $Zn_{0.7}Mn_{0.3}S$, (d) $Zn_{0.5}Mn_{0.5}S$, (e) $Zn_{0.4}Mn_{0.6}S$. (The zero energy corresponds to 1023.5 eV.)

selected at the inflection point of the edge; the Zn L_{II} edge is located ~22 eV above the L_{III} edge. The most noticeable result found in Fig. 1 is a dramatic reduction of feature A, located just above the L_{III} edge, with increasing Mn concentration in the alloys. Conversely, feature B, which is centered around 10.5 eV relative to the L_{III} edge, decreases only slightly in magnitude with increasing Mn content in the alloys. We attribute the main feature of the near-edge region (peak A) in Fig. 1 to dipole-allowed transitions of photoelectrons from Zn $2p$ states to a relatively narrow unoccupied $3d$ band, which occurs from Zn $3d$–S $3p$ hybridized states. Peak A is clearly sharpest for ZnS, becoming progressively broader, while shifting slightly towards higher energy, with increasing Mn content in $Zn_{1-x}Mn_xS$ alloys; the energy shift of peak A is approximately 1 eV for $Zn_{0.5}Mn_{0.5}S$ relative to ZnS. This can be explained by noting that the Zn $3d$–S $3p$ hybridized electronic states are situated between Zn $3d$ and S $3p$ states, these being more localized in ZnS than in $Zn_{1-x}Mn_xS$ alloys. This shows that Mn ions directly influence the local density of Zn unoccupied $3d$ states while substituting for Zn in $Zn_{1-x}Mn_xS$. Wei and Zunger[9] have calculated the energy levels of Zn $3d$ states in Mn-based DMS alloys using tight-binding theory and found that they are situated further away in energy from the S $3p$ states than are the Mn $3d$ states, implying that the Mn $3d$ states have higher hybridization probability with the S $3p$ states in comparison with the Zn $3d$ states. We believe that, upon substitution in the cation sublattice in $Zn_{1-x}Mn_xS$, Mn ions not only reduce the number of unoccupied S $3p$–Zn $3d$ states but also add unoccupied S $3p$–Mn $3d$ states, thereby causing a decrease in intensity of peak A with increased Mn concentration x in

$Zn_{1-x}Mn_xS$. This is in agreement with a generally accepted rule that hybridization effects in transition-metal oxides are relatively smaller in the late-transition- than in the early transition-metal oxides[10] and earlier theoretical studies in which it was shown that Mn substitution increases *p-d* hybridization effects in DMS alloys.[2,3]

In a similar fashion as for peak *A*, there is an energy shift for feature *B* of approximately 1 eV for $Zn_{0.5}Mn_{0.5}S$ relative to ZnS. The likelihood is that feature *B* is not a resonance peak but that it is due to dipole-allowed transitions of photoelectrons from Zn 2*p* states to continuum states having primarily *d*-orbital character.

Sulfur *K*-edge XANES spectra

Figures 2–4 show the S *K*-edge XANES spectra for the $Zn_{1-x}M_xS$ (M = Mn,Fe,Co) systems. After pre-edge background subtraction, the spectra have been normalized to unity at the absorption edge, which was assigned at the first inflection point above the threshold. There appears to be a very weak peak occurring at −4 to −5 eV. However, due to insufficient signal intensity in comparison to the noise, we are unable to confirm this. The alloys' XANES spectra reveal a most interesting linear increase in the intensity of the pre-edge feature *A*, located from 0.5 to 2 eV below the edge, with increasing transition-metal content; the feature is absent in the ZnS S *K*-edge spectra. As far as we know, this is the first observation of such a phenomenon for any alloy system. We observe an increase in overall intensity of pre-edge feature *A* with increasing atomic number *Z* of the substitutional transition-metal element: The feature appears to be best resolved and have the highest intensity for the $Zn_{1-x}Co_xS$ system and least resolved with lowest intensity for $Zn_{1-x}Mn_xS$ alloys. This is demonstrated in a more forthright fashion using Figs. 5–7. These figures show the normalized ZnS S *K*-edge spectra subtracted from similar spectra for the alloys. A monotonically increasing background with energy appears in these figures as a result of our choice of normalization. We believe

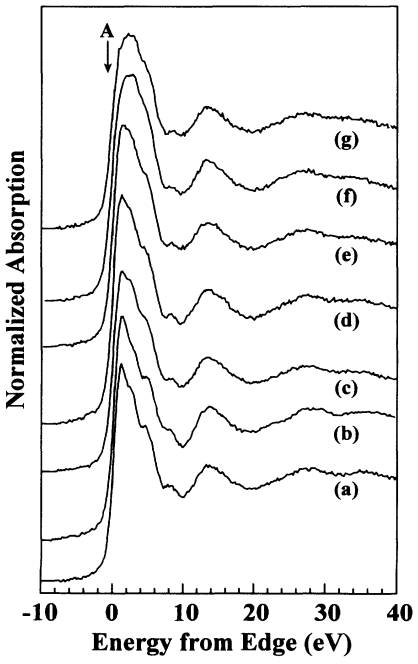

FIG. 2. Normalized S *K* near-edge absorption spectra. (a) ZnS, (b) $Zn_{0.95}Mn_{0.05}S$, (c) $Zn_{0.9}Mn_{0.1}S$, (d) $Zn_{0.8}M_{0.2}S$, (e) $Zn_{0.7}Mn_{0.3}S$, (f) $Zn_{0.5}Mn_{0.5}S$, (g) $Zn_{0.4}Mn_{0.6}S$. (The zero energy corresponds to 2472.5 eV.)

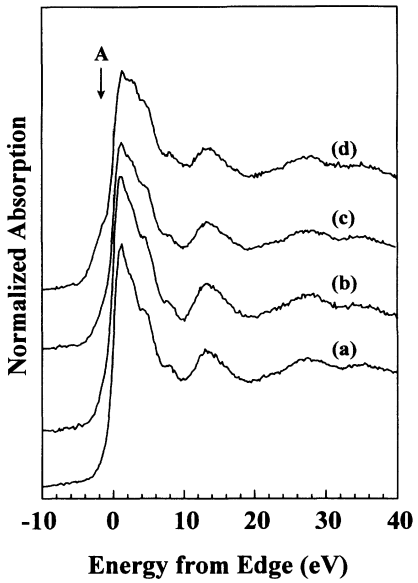

FIG. 3. Normalized S *K* near-edge absorption spectra. (a) $Zn_{0.9}Fe_{0.1}S$, (b) $Zn_{0.8}Fe_{0.2}S$, (c) $Zn_{0.7}Fe_{0.3}S$, (d) $Zn_{0.5}Fe_{0.5}S$.

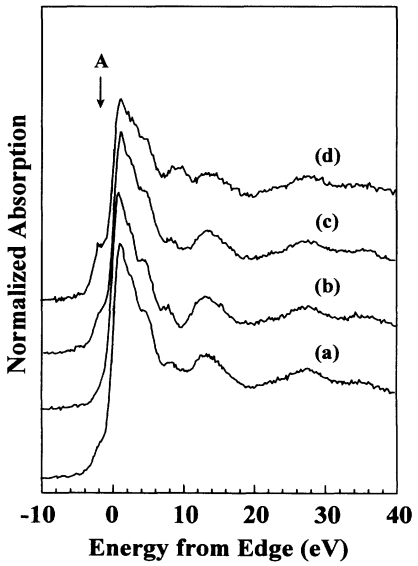

FIG. 4. Normalized S *K* near-edge absorption spectra. (a) $Zn_{0.95}Co_{0.05}S$, (b) $Zn_{0.9}Co_{0.1}S$, (c) $Zn_{0.7}Co_{0.3}S$, (d) $Zn_{0.5}Co_{0.5}S$.

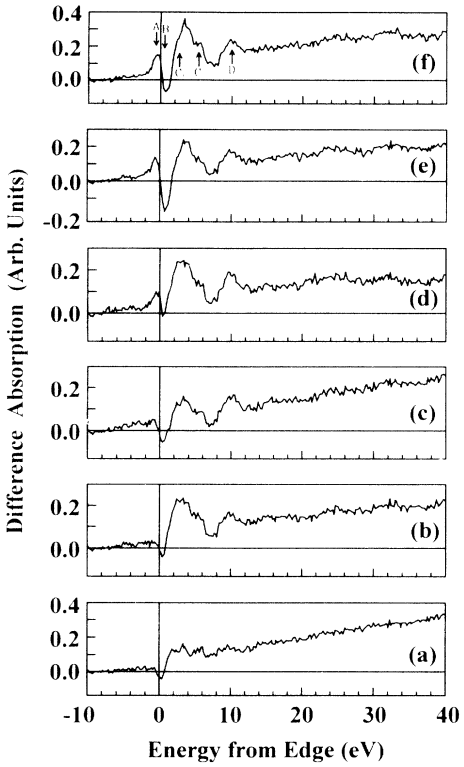

FIG. 5. "Difference" S K near-edge absorption spectra calculated using $Zn_{1-x}Mn_xS-ZnS$. (a) $Zn_{0.95}Mn_{0.05}S$, (b) $Zn_{0.9}Mn_{0.1}S$, (c) $Zn_{0.8}Mn_{0.2}S$, (d) $Zn_{0.7}Mn_{0.3}S$, (e) $Zn_{0.5}Mn_{0.5}S$, (f) $Zn_{0.4}Mn_{0.6}S$. (The zero energy corresponds to 2472.5 eV.)

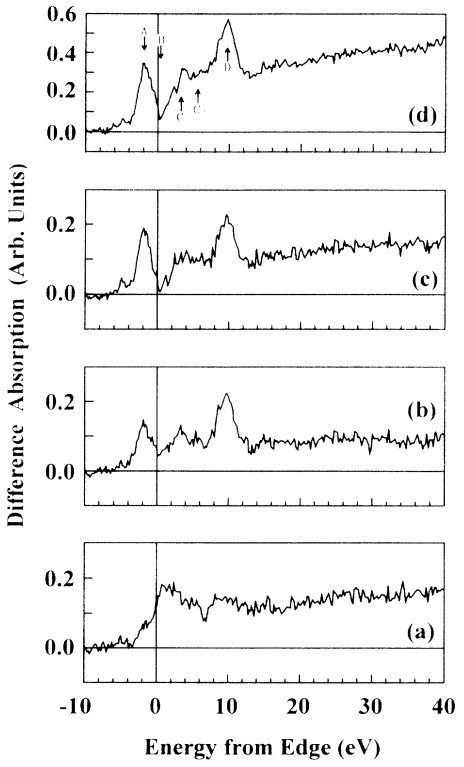

FIG. 7. "Difference" S K near-edge absorption spectra calculated using $Zn_{1-x}Co_xS-ZnS$. (a) $Zn_{0.95}Co_{0.05}S$, (b) $Zn_{0.9}Co_{0.1}S$, (c) $Zn_{0.7}Co_{0.3}S$, (d) $Zn_{0.5}Co_{0.5}S$.

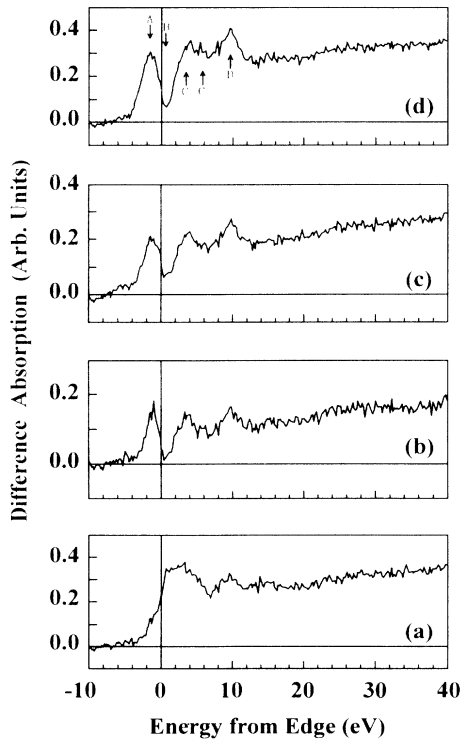

FIG. 6. "Difference" S K near-edge absorption spectra calculated using $Zn_{1-x}Fe_xS-ZnS$. (a) $Zn_{0.9}Fe_{0.1}S$, (b) $Zn_{0.8}Fe_{0.2}S$, (c) $Zn_{0.7}Fe_{0.3}S$, (d) $Zn_{0.5}Fe_{0.5}S$.

that the pre-edge peak A of the XANES spectra for all $Zn_{1-x}M_xS$ alloys can be attributed to a photoelectron transition from S $1s$ to S $3p$–transition-metal (Mn,Fe,Co) $3d(t_2)$ hybridized states. A similar assignment to a pre-edge peak for S K-edge $CuFeS_2$ XANES data was made by Petiau, Sainctavit, and Calas,[11] although the symmetry of the Fe $3d$ states hybridizing with S $3p$ states was not identified.

There are two potential concerns regarding our interpretation of pre-edge peak A of the S K-edge spectra for our $Zn_{1-x}M_xS$ alloys which require addressing: (1) the influence of intrinsic and instrumental broadening of the near-edge structure, and (2) final-state effects, such as core excitations or shakeoff processes. Core-hole broadening can be of order 0.5 eV, and in some systems has been shown to depend upon the state of aggregation of the absorbing element.[12] However, as discussed in the last section, the instrumental broadening for these measurements ranges from 0.5 to 1.2 eV. The intrinsic broadening due to the excited-state lifetime of the S K-edge core vacancy is calculated to be 0.59 eV,[13] which is about a factor of 2 less than the monochromator resolution at that energy. Although final-state processes are known to contribute to broadening,[14] this contribution is also small with respect to the instrumental broadening. Similarly, excitonic effects may be estimated by their binding energy, which are calculated to be of the order of 100 meV or less,[15] also much smaller than the monochromator resolution. We conclude that lifetime and final-

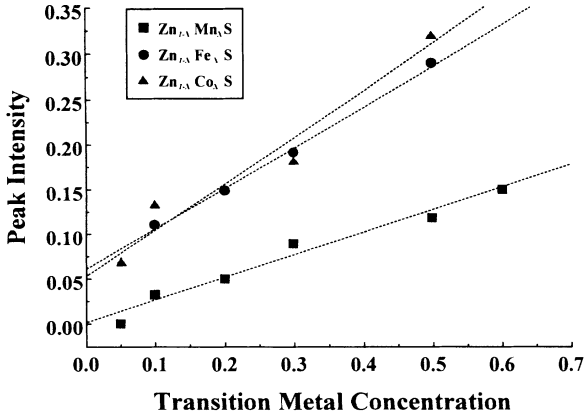

FIG. 8. Pre-edge peak A intensity and fit using linear regression as a function of transition-metal concentration for $Zn_{1-x}Mn_xS$, $Zn_{1-x}Fe_xS$, and $Zn_{1-x}Co_xS$ alloys.

state effects, while present, are obscured by the instrumental resolution and are not responsible for the observed near-edge structure.

In order to determine systematically its concentration dependence, we have calculated the intensity of peak A from the difference spectra (alloy spectra $-$ZnS spectra) for the three types of alloys and plotted our results as a function of x in Fig. 8. We find that, within the concentration ranges we have studied (0.05–0.6), the dependence of the intensity of peak A on x is linear. Furthermore, the rate of increase in intensity of peak A with x is dependent upon the type of substitutional transition-metal ion; the rate of increase is greatest for $Zn_{1-x}Co_xS$ alloys and least for $Zn_{1-x}Mn_xS$ alloys. Peak A intensities for the alloys are recorded in Table I and the linear-regression slope values are recorded in Table II. It is not known to what extent the intercepts are a result of improper normalization procedure or a nonlinear x dependence of peak A intensity for lower concentrations of transition metal. The linear x dependence of peak A intensity can be understood in the following manner. The transition probability for the S $1s$ to S $3p-M$ $3d(t_2)$ excitation is a function of the availability of such states, this in turn being reflected in the density-of-states (DOS)

TABLE I. Intensity of the pre-edge feature peak A, calculated from the "difference" spectra ($Zn_{1-x}M_xS-ZnS$) measured at the S K edge for $Zn_{1-x}Mn_xS$, $Zn_{1-x}Fe_xS$, and $Zn_{1-x}Co_xS$ alloys.

x	$Zn_{1-x}Mn_xS$	$Zn_{1-x}Fe_xS$	$Zn_{1-x}Co_xS$
0.05	0.00±0.01		0.07±0.01
0.1	0.03±0.01	0.11±0.02	0.13±0.01
0.2		0.15±0.02	
0.3	0.09±0.01	0.19±0.02	0.18±0.02
0.5	0.12±0.01	0.29±0.02	0.32±0.02
0.6	0.15±0.02		

TABLE II. Slope and intercept of the line fitted using linear regression to the intensity of the pre-edge feature peak A as a function of concentration from S K-edge XANES spectra for $Zn_{1-x}Mn_xS$, $Zn_{1-x}Fe_xS$, and $Zn_{1-x}Co_xS$ alloys.

	$Zn_{1-x}Mn_xS$	$Zn_{1-x}Fe_xS$	$Zn_{1-x}Co_xS$
Slope	0.25±0.01	0.45±0.01	0.51±0.03
Intercept	0.00±0.01	0.06±0.01	0.05±0.02

features for the material. The DOS associated with the S $1s$ to S $3p-M$ $3d(t_2)$ hybridized states increases with x because proportionally more transition-metal $3d(t_2)$ orbitals become available for hybridization with S $3p$ orbitals.

As shown in Table II, the rate of increase in peak A intensity with x for $Zn_{1-x}Co_xS$ and $Zn_{1-x}Fe_xS$ alloys is about twice as much as for $Zn_{1-x}Mn_xS$ alloys, with the highest rate occurring for Co-based DMS's. This result is most interesting because it reveals fundamental aspects of p-d hybridization occurring in $Zn_{1-x}M_xS$ alloys. This can be explained with greater clarity using Fig. 9, which shows a schematic representation of the Mn, Fe, or Co $3d$ bands of $Zn_{1-x}M_xS$ alloys derived from their respective atomic levels. Our model is in part based on earlier photoemission results for $Cd_{1-x}Fe_xSe$ alloys by Taniguchi *et al.*[16] and most closely resembles a model derived from band-structure calculations for $Cd_{1-x}Mn_xTe$ alloys by Wei and Zunger:[17] the main difference between them is that Wei and Zunger locate the Mn $3d(e)$ band just above the bottom of the conduction band whereas Taniguchi *et al.* place the Fe $3d(e)$ band just below the top of the valence band. The model shown in Fig. 9 is given added support from our recent Mn, Fe, and Co L_{III}- and L_{II}-edge XANES measurements for $Zn_{1-x}M_xS$ alloys.[18]

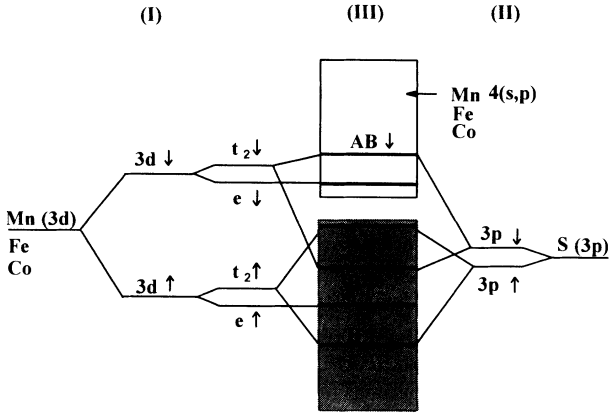

FIG. 9. Schematic energy diagram showing respective atomic levels forming M $3d$ bands (M =Mn,Fe,Co) and $Zn_{1-x}M_xS$ alloys. (I) Exchange and crystal-field splitting of Mn, Fe, and Co $3d$ states, (II) Exchange splitting of S $3p$ states, and (III) the final hybridized states. AB and B denote antibonding and bonding states, respectively. ↑ and ↓ denote states for spin up and spin down, respectively (not to scale).

Referring to Fig. 9, our assignment for peak A can be made more specific; since, by symmetry arguments, photoelectrons originating from s states become excited to the first empty p-like states above the Fermi level, the most reasonable conclusion is that peak A corresponds to $1s$ electrons making transitions to a narrow band of M $3d(t_2\downarrow)$–S $3p(\downarrow)$ hybridized antibonding states. As shown by several groups having performed electronic band-structure calculations,[19–21] the S $3p$ states participate in hybridization with Zn $4(s,p)$ states in ZnS and the resulting band structure has the first p band of empty states approximately 4 eV above (at Γ) the bottom of the conduction band.[11] The strength of p-d hybridization in $Zn_{1-x}M_xS$ alloys, which is determined by the extent to which S $3p$- and M $3d$-orbital wave functions overlap, is reflected in the DOS. As a result, the rate of change of peak A intensity with concentration for these alloys is directly proportional to the strength of p-d hybridization. Our results indicate that S $3p$–$M3d$ hybridization is strongest for $Zn_{1-x}Co_xS$ and weakest for $Zn_{1-x}Mn_xS$. This is consistent with magnetic susceptibility[22] and neutron scattering studies[23] which indicate a significantly larger nearest-neighbor exchange integral for $Zn_{1-x}Co_xS$ than for $Zn_{1-x}Mn_xS$.

We have estimated the energies at which peak A is positioned in the spectra for the alloys using the mean value of the smoothed peak profile and tabulated these in Table III. Peak A is found slightly lower in energy (0.3 eV) for $Zn_{1-x}Co_xS$ than for $Zn_{1-x}Fe_xS$ and substantially lower (1.4 eV) than for $Zn_{1-x}Mn_xS$. Therefore the relative location in energy of the S $3p$–$M3d(t_2)$ hybridized band for $Zn_{1-x}M_xS$ alloys depends directly on the atomic number of the substitutional transition-metal ion. Although we believe that the selected position of the absorption edge will determine the value in Table III, in the meanwhile, the position of the inflection point of an absorption edge does not bear a unique relationship to the Fermi-energy location. However, the pre-edge peaks A were well separated from the threshold, and the additional dashed line in Figs. 2–4 (S K edge) is only to clarify how the edge energy is chosen. In reality, it has no effect on the analysis of the above discussions.

In contrast to the trend for peak A, there is a relative decrease in intensity with x of the first above-edge feature, peak B located less than 1 eV above the edge; this is best seen from Figs. 5–7. Qualitatively, the magnitude of reduction of this peak with x appears to be the same for all three systems. Sainctavit *et al.*[24] have previously made S K-edge XANES studies of ZnS and have assigned the first above-edge peak to transitions of the photoelectron from the S $1s$ state to S $3p$–Zn$4(s,p)$ hybridized states. When evaluated in conjunction with one another, both the increase of peak A and the corresponding decrease in intensity of the above-edge peak B with x are consistent with more S $3p$–transition-metal $3d(t_2)$ hybridized states and less S $3p$–Zn $4(s,p)$ hybridized states becoming available as transition-metal content increases in the alloys. This is reasonable since some of the S $3p$ states originally hybridizing with Zn $4(s,p)$ states in ZnS hybridize with transition-metal $3d(t_2)$ states in $Zn_{1-x}M_xS$ alloys. The position of peak B is found to be nearly the same for $Zn_{1-x}Mn_xS$ and $Zn_{1-x}Fe_xS$ (approximately 0.5–0.6 eV above the edge) while for $Zn_{1-x}Co_xS$ it is located approximately 0.3 eV closer in energy to the edge. This may be indicative of the difference in the DOS profile between the three alloy systems.

TABLE III. Position in energy, relative to the S K-edge value of 2472.5 eV, for identifiable features from the XANES spectra of $Zn_{1-x}Mn_xS$, $Zn_{1-x}Fe_xS$, and $Zn_{1-x}Co_xS$ alloys. The features are identified with arrows on Figs. 5–7.

Feature	$Zn_{1-x}Mn_xS$ (eV)	$Zn_{1-x}Fe_xS$ (eV)	$Zn_{1-x}Co_xS$ (eV)
A	−0.5±0.1	−1.6±0.2	−1.9±0.2
B	0.6±0.2	0.5±0.2	0.2±0.1
C_1	3.3±0.3	3.5±0.3	3.2±0.3
C_2	5.5±0.3	5.8±0.3	5.6±0.3
D	9.8±0.3	9.8±0.3	9.8±0.3

While systematic trends are difficult to ascertain, peaklike features C_1, C_2, and D, all occurring below 10 eV above the edge, are generally found to increase in intensity upon substitution of transition-metal ions for Zn ions in ZnS: Their energy locations in the alloys' spectra are tabulated in Table III. Similar conclusions as for peak B are drawn for these features.

IV. CONCLUSIONS

Our results indicate a significant effect on the DOS features associated with photoelectron excitations of $Zn_{1-x}M_xS$ alloys due to transition-metal $3d$–S $3p$ orbital hybridization. The most striking of these is a concentration- and transition-metal-type-dependent pre-edge peak associated with transitions to a hybridized band of M $3d(t_2)$–S $3p$ antibonding states. This feature was found to increase linearly in intensity with concentration for the alloys, in proportion to the strength of the M $3d(t_2)$–S $3p$ hybridization. From its location in the XANES spectra, we conclude that the location in energy of the hybridized band of M $3d(t_2)$–S $3p$ antibonding states for $Zn_{1-x}M_xS$ alloys depends directly on the atomic number of the transition-metal ion. To our knowledge, this is the first time that a detailed study of both concentration and substitutional-ion-type dependence of XANES for an alloy system has been made.

ACKNOWLEDGMENTS

We thank Professor J. K. Furdyna and U. Debska for providing the samples used in this study. This work was supported in part by the National Science Council of the R.O.C., under Contract No. NSC82-0208-M-032-016. This work was performed on beamline 7A at UVSOR, the Institute for Molecule Science (IMS).

[1] *Diluted Magnetic Semiconductors,* edited by J. K. Furdyna and J. Kossut, Semiconductors and Semimetals Vol. 25 (Academic, New York, 1988); *Diluted Magnetic Semiconductors,* edited by M. Jain (World Scientific, Singapore, 1991).

[2] B. E. Larson, K. C. Hass, H. Ehrenreich, and A. E. Carlsso, Solid State Commun. **56**, 347 (1985); K. C. Hass, B. E. Larson, H. Ehrenreich, and A. E. Carlsso, J. Magn. Magn. Mater. **54-57**, 1283 (1986).

[3] B. E. Larson, K. C. Hass, H. Ehrenreich, and A. E. Carlsso, Phys. Rev. B **37**, 4137 (1988).

[4] J. Spalek, A. Lewicki, Z. Tarnawski, J. K. Furdyna, R. R. Galazka, and Z. Obuszko, Phys. Rev. B **33**, 3407 (1986).

[5] W. F. Pong, R. A. Mayanovic, B. A. Bunker, J. K. Furdyna, and U. Debska, Phys. Rev. B **41**, 8440 (1990).

[6] R. A. Mayanovic, W. F. Pong, and B. A. Bunker, Phys. Rev. B **42**, 11 174 (1990).

[7] P. J. Durham, in *X-ray Absorption, Principles, Techniques, Applications of EXAFS, SEXAFS and XANES,* edited by R. Prins and D. C. Koningsberger (Wiley, New York, 1986).

[8] A. Bianconi, Appl. Surf. Sci. **6**, 392 (1980); in *X-ray Absorption, Principles, Techniques, Applications of EXAFS, SEXAFS and XANES* (Ref. 7).

[9] S. H. Wei and A. Zunger, Phys. Rev. B **37**, 8958 (1988).

[10] F. M. F. deGroot, M. Grioni, J. C. Fuggle, J. Ghijsen, G. A. Sawatzky, and H. Petersen, Phys. Rev. B **40**, 5715 (1989).

[11] J. Petiau, Ph. Sainctavit, and G. Calas, Mater. Sci. Eng. B **1**, 237 (1988).

[12] N. J. Shevchik, Phys. Rev. Lett. **33**, 1336 (1974).

[13] M. O. Krause and J. H. Oliver, J. Phys. Chem. Ref. Data **8**, 329 (1979).

[14] P. C. Kemeny and N. J. Shevchik, Solid State Commun. **17**, 255 (1975).

[15] C. Kittel, *Introduction to Solid State Physics* (Wiley, New York, 1986), p. 298.

[16] M. Taniguchi, Y. Ueda, I. Morisada, Y. Murashita, T. Ohta, I. Souma, and Y. Oka, Phys. Rev. B **41**, 3069 (1990).

[17] S. H. Wei and A. Zunger, Phys. Rev. B **35**, 2340 (1987).

[18] W. F. Pong *et al.* (unpublished).

[19] P. Eckelt, Phys. Status Solidi **23**, 307 (1967).

[20] C. S. Wang and B. M. Klein, Phys. Rev. B **24**, 3393 (1981).

[21] J. E. Bernard and A. Zunger, Phys. Rev. B **36**, 3199 (1987).

[22] A. Lewicki, A. I. Schindler, J. K. Furdyna, and W. Giriat, Phys. Rev. B **40**, 2379 (1989).

[23] T. M. Giebultowicz, P. Klosowski, J. J. Rhyne, T. J. Udovic, J. K. Furdyna, and W. Giriat, Phys. Rev. B **41**, 504 (1990).

[24] Ph. Sainctavit, J. Petiau, A. M. Flank, J. Ringeissen, and S. Lewonczuk, Physica B **158**, 623 (1989).

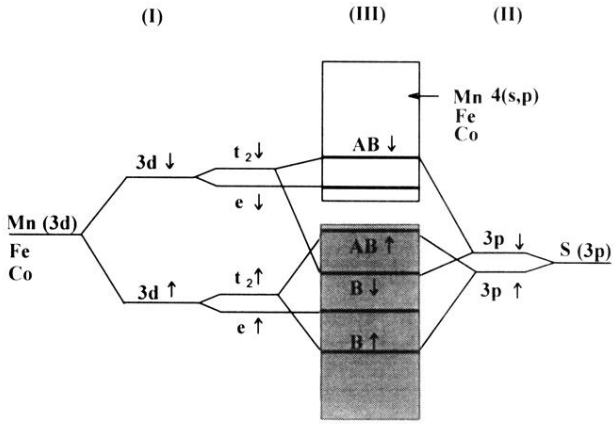

FIG. 9. Schematic energy diagram showing respective atomic levels forming M 3d bands (M = Mn,Fe,Co) and $Zn_{1-x}M_xS$ alloys. (I) Exchange and crystal-field splitting of Mn, Fe, and Co 3d states, (II) Exchange splitting of S 3p states, and (III) the final hybridized states. AB and B denote antibonding and bonding states, respectively. ↑ and ↓ denote states for spin up and spin down, respectively (not to scale).